Available online at www.sciencedirect.com

SciVerse ScienceDirect

Journal of the European Ceramic Society 32 (2012) 2389–2397

www.elsevier.com/locate/jeurceramsoc

Structural, dielectric, and piezoelectric properties of fine-grained NBT–$BT_{0.11}$ ceramic derived from gel precursor

Marin Cernea [a,*], Carmen Galassi [b], Bogdan S. Vasile [c], Claudio Capiani [b], Ciceron Berbecaru [d], Ioana Pintilie [a], Lucian Pintilie [a]

[a] *National Institute of Materials Physics, P.O. Box MG-7, Bucharest-Magurele 077125, Romania*
[b] *National Research Council – Institute of Science and Technology for Ceramics, Via Granarolo 64, I-48018 Faenza, Italy*
[c] *University POLITEHNICA of Bucharest, 060042, Romania*
[d] *University of Bucharest, 70709 Bucharest, Romania*

Received 29 September 2011; received in revised form 30 January 2012; accepted 1 February 2012
Available online 7 March 2012

Abstract

$(Na_{1/2}Bi_{1/2})TiO_3$ doped *in situ* with 11 mol% $BaTiO_3$ (NBT–$BT_{0.11}$) powders were synthesized by a sol–gel method, and the electrical properties of the resulting ceramics were investigated. The powders consisting of uniform and fine preliminary particles of about 50 nm were prepared by calcining the gel precursor at 700 °C. $(Na_{1/2}Bi_{1/2})_{0.89}Ba_{0.11}TiO_3$ ceramics, sintered at temperatures up to 1150 °C have a rhombohedral symmetry, while the ceramic sintered at 1200 °C exhibits a tetragonal crystalline structure. The ceramics show high dielectric constant ($\varepsilon_r \sim 5456$), dielectric loss of 0.02, depolarization temperature $T_d \sim 110$ °C and temperature corresponding to the maximum value of dielectric constant $T_m \sim 262$ °C. The dielectric constant (ε_{33}) and the piezoelectric constant (d_{33}) attain the maximum values of 924 and 13 pC/N, respectively, while the electromechanical coupling factor (k_p) value is 0.035. The NBT–$BT_{0.11}$ ceramics derived from sol–gel present high mechanical quality factor ($Q_m \sim 860$). The dielectric and piezoelectric properties values of NBT–$BT_{0.11}$ ceramics derived from sol–gel are smaller than those of samples produced by the conventional solid state reaction method, due to the grains size and oxygen vacancies that generate dipolar defects.

Keywords: A. Sol–gel processes; C. Dielectric properties; C. Piezoelectric properties; D. $BaTiO_3$ and titanates

1. Introduction

Lead zirconate titanate (PZT) ceramics exhibit excellent electric properties and are extensively used in numerous electronic devices, such as actuators, sensors, capacitors, and high-power transducers.[1,2] On the other hand, PZT ceramics have been continuously modified with different additives, which make them more attractive for specific applications. Thus, incorporating ZnO to PZT ceramics contributes to an obvious improvement of the fracture properties.[3] ZnO whiskers and Sb_2O_3 co-modified lead zirconate titanate composites show enhanced piezoelectric and mechanical properties,[4] while Nb_2O_5 enhance piezoelectric and ferroelectric properties of the monolithic PZT.[5]

With the increasing environmental concerning, lead-free piezoelectric ceramics have turned to be a certain trend in the sustainable development. Lead-free piezoelectric materials include $BaTiO_3$, $(Na,Bi)TiO_3$, $(Na,K)NbO_3$ system and so on.[6]

$Na_{1/2}Bi_{1/2}TiO_3$ (NBT) is a ferroelectric compound with perovskite structure and rhombohedral symmetry.[7] Usually, the NBT ceramic exhibits weak piezoelectric properties.[8] In order to improve the piezoelectric properties of this ceramic, a large number of NBT-based solid solutions, including NBT–$BaTiO_3$ (NBT–BT), have been prepared and intensively studied in recent years.[9–20] The partial substitution of $(Na_{0.5}Bi_{0.5})^{2+}$-site ions by Ba^{2+} contributes to the decrease of Curie temperature and to the improvement of sintering and piezoelectric properties. The $(1-x)$NBT–xBT (abbreviated as NBT–BT_x) ceramics with 1–20 mol% $BaTiO_3$ were studied. NBT–BT_x system has attracted considerable attention, because of the existence of a rhombohedral–tetragonal morphotropic phase boundary (MPB) near $x = 0.06$. Compositions close to the MPB provide

* Corresponding author. Tel.: +40 21 369 01 70x130; fax: +40 21 369 01 77.
E-mail address: mcernea@infim.ro (M. Cernea).

0955-2219/$ – see front matter © 2012 Elsevier Ltd. All rights reserved.
doi:10.1016/j.jeurceramsoc.2012.02.021

substantially improved poling and piezoelectric properties.[18,21] Similar to pure NBT, NBT–BT_x ($x < 0.06$) ceramic has a rhombohedral perovskite structure. As x increases, a tetragonal phase appears and increases continuously. At $x \sim 0.10$, the ceramic becomes a pure tetragonal phase. These suggest that a MPB of rhombohedral and tetragonal phases resides for $0.06 < x < 0.10$.[7] In this paper, we investigated the piezoelectric properties of NBT–BT_x ($x = 0.11$) ceramic outside the MPB domain, where this ceramic should present a tetragonal structure.

NBT-based ceramics are usually fabricated by the conventional solid-state method. Recently, considerable research efforts have been devoted to the preparation of materials by various wet chemical methods, such as citrate method,[22,23] emulsion method,[24] hydrothermal process,[25] sol–gel techniques[26,27] and stearic acid gel route.[28] It was found that NBT-based ceramics made from powders synthesized by alternative methods exhibit improved sinterability, poling process and piezoelectric properties. In the present study, NBT–$BT_{0.11}$ ceramics were produced by the sol–gel method, and their structure and electrical properties were examined.

2. Experimental procedures

Precursor sol of $0.89[(Na_{0.5}Bi_{0.5})TiO_3]$–$0.11[BaTiO_3]$ was prepared by a sol–gel technique starting from sodium acetate [$Na(CH_3COO)$], barium acetate [$Ba(CH_3COO)_2$], bismuth (III) acetate [$Bi(CH_3COO)_3$] and titanium (IV) isopropoxide, 97% solution in 2-propanol [$Ti\{OCH(CH_3)_2\}_4$], acetic acid and isopropanol. All reagents (Aldrich) are of analytical grade purity. The procedure is described in detail in a previous publication.[27] After drying the gel at 100 °C, the resulting powder was treated at different temperatures in order to obtain a single-phase powder. The ceramic samples were prepared by uniaxial pressing at 100 MPa. The as-obtained pellets with 10 mm diameter and 1 mm thickness were then sintered at various temperatures, in the 1100–1200 °C range, for 1 h, in air. Samples with apparent densities of 94–96% of the theoretical density were obtained. The calcined powder was investigated by scanning and transmission electronic microscopy (SEM, TEM) and X-ray diffraction (XRD). The microstructure of the samples was investigated using a FEI Quanta Inspect F scanning electron microscope and a Tecnai^{TM} G^2 F30 S-TWIN transmission electron microscope with a line resolution of 1 Å, in high resolution transmission electron microscopy (HR-TEM) mode and selected area electron diffraction (SAED). For diffraction analysis, a Bruker-AXS tip D8 ADVANCE diffractometer with Cu $K_{\alpha 1}$ radiation (wavelength 1.5406 Å), LiF crystal monochromator and Bragg–Brentano diffraction geometry was used. The data were acquired at 25 °C, with a step-scan interval of 0.020° and a step time of 10 s. The electrical measurements were carried out in the metal-ferroelectric-metal (MFM) configuration, where the electrodes M consist of silver. Dielectric measurements at fixed frequencies in the 120 Hz to 1 MHz frequency intervals have been performed on a temperature range between room temperature of about 25 °C and 300 °C. A Hioki 3532-50 type automatic RLC bridge and Kethley 2000 voltmeter, with chromel–alumel thermocouple type for temperature measurements, were controlled by a computer through the GPIB interfaces for automatic experimental data registration and further investigations. P–E loops were measured using a Radiant (Premier II) System. For the piezoelectric measurements, the samples were poled under an applied field of 3 kV/mm, at 120 °C, for 40 min. Piezoelectric properties were measured by a resonance-antiresonance method on the basis of IEEE 176-1987 standards, using an impedance analyzer (HP 4194A). The electromechanical coupling factor (k_{33}), was calculated from the resonance and antiresonance frequencies. The dielectric constant (ε_{ii}^{T}), was determined from the capacitance of the poled specimen at 1 kHz. The elastic constants (s_{jj}^{E}), was calculated using the frequency constant (N_{ij}) and the measured density (ρ_o), by the relation $s_{11}^{E} = 10^9/(^2N_P^2\rho_o)$. Finally, the piezoelectric constants (d_{ij}) were calculated using the k_{ij}, ε_{ii}^{T} and s_{jj}^{E} values, by the equation

$$d_{ij} = k_{ij}(\varepsilon_{ii}^{T} s_{jj}^{E})^{1/2}.$$

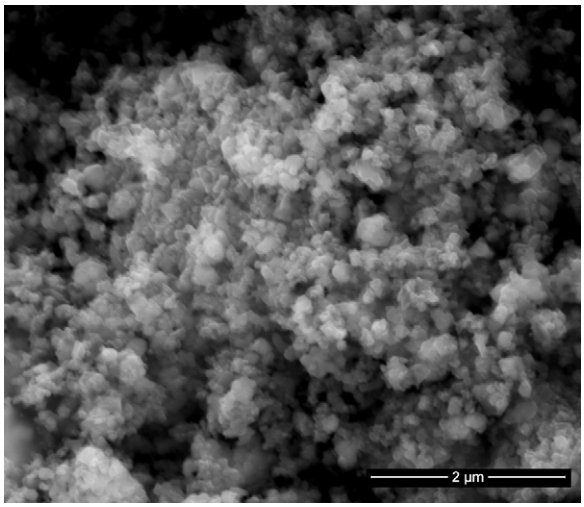

Fig. 1. SEM photomicrograph of 11 mol%$BaTiO_3$ doped-$Na_{1/2}Bi_{1/2}TiO_3$ precursor gel, heated at 700 °C, 3 h.

3. Results and discussion

3.1. Microstructure

The SEM micrograph of $Na_{0.5}Bi_{0.5}TiO_3$ doped with 11 mol% $BaTiO_3$ powder calcined at 700 °C, 3 h, in air, is presented in Fig. 1.

It can be seen that the sol–gel derived powder has a regular morphology, as a result of the agglomeration of preliminary particles of 40–60 nm.

The TEM and HR-TEM images and SAED pattern of the powder calcined at 700 °C, 3 h, in air, are shown in Fig. 2. The TEM image (see Fig. 2(a)) reveals that the powder is composed of spherical and polyhedral particles with the tendency to form agglomerates; the average size of the nanocrystallites is about 50 nm.

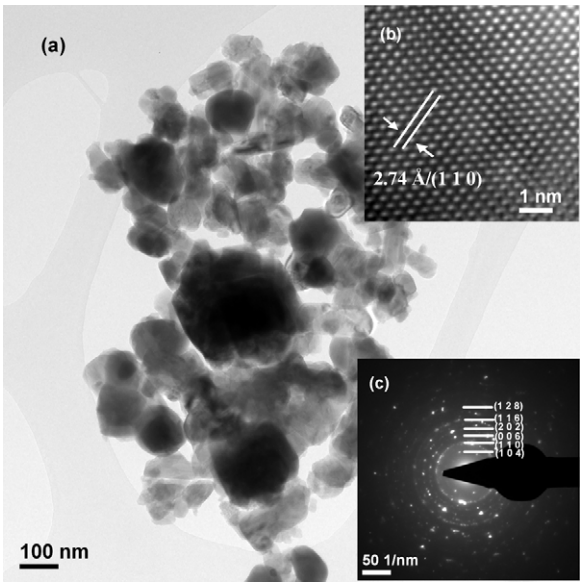

Fig. 2. TEM images of $BaTiO_3$ doped-$Na_{1/2}Bi_{1/2}TiO_3$ precursor gel heated at 700 °C (a). The insets present images of corresponding HR-TEM (b) and SAED (c) of NBT–$BT_{0.11}$ nanocrystals.

Fig. 2(b) shows clear lattice fringes with $d = 2.74$ Å corresponding to the (1 1 0) crystallographic planes of rhombohedral $Ba_{0.5}Na_{0.5}TiO_3$. The regular succession of the atomic planes indicates that the crystallites are structurally uniform, without point defects. By analyzing the selected area diffraction pattern shown in Fig. 2(c), we can state that the only phase identified is the rhombohedral phase of $Na_{0.5}Ba_{0.5}TiO_3$.[29]

3.2. Structure

The XRD patterns ($2\theta = 20$–$80°$) of the powder and pellets prepared for this study are presented in Fig. 3(a). Fig. 3(b) shows the XRD patterns of the powder and ceramics in the 38–48° 2θ range.

A main phase with perovskite structure and traces of a secondary phase are observed for the samples calcined at temperatures up to 1150 °C. There are only some little differences between the patterns. The rhombohedral symmetry of NBT–$BT_{0.11}$ ceramic at room temperature can be characterized by a (0 0 3)/(0 2 1) peak splitting between 39° and 41° and a single (2 0 2) peak between 45° and 48°. The rhombohedral (0 0 3)/(0 2 1) peak splitting conserves until the temperature reaches 1150 °C and then is replaced by the (1 1 1) peak at 1200 °C. This result contradicts Ref. 7, which suggests that the MPB of rhombohedral and tetragonal phases resides for $0.06 < x < 0.10$ and the NBT–BT_x ceramic becomes a pure tetragonal phase for $x \sim 0.10$. The crystal structure of NBT–$BT_{0.11}$ ceramics sintered at 1200 °C exhibits a degree of tetragonality corresponding to the splitting of the (2 0 0) and (0 0 2) characteristic peaks at $2\theta \sim 46.5°$. These results suggest that the rhombohedral–tetragonal phase transition of NBT–$BT_{0.11}$ ceramics takes place at 1200 °C sintering temperature. It is known that grain size can have an important influence on the

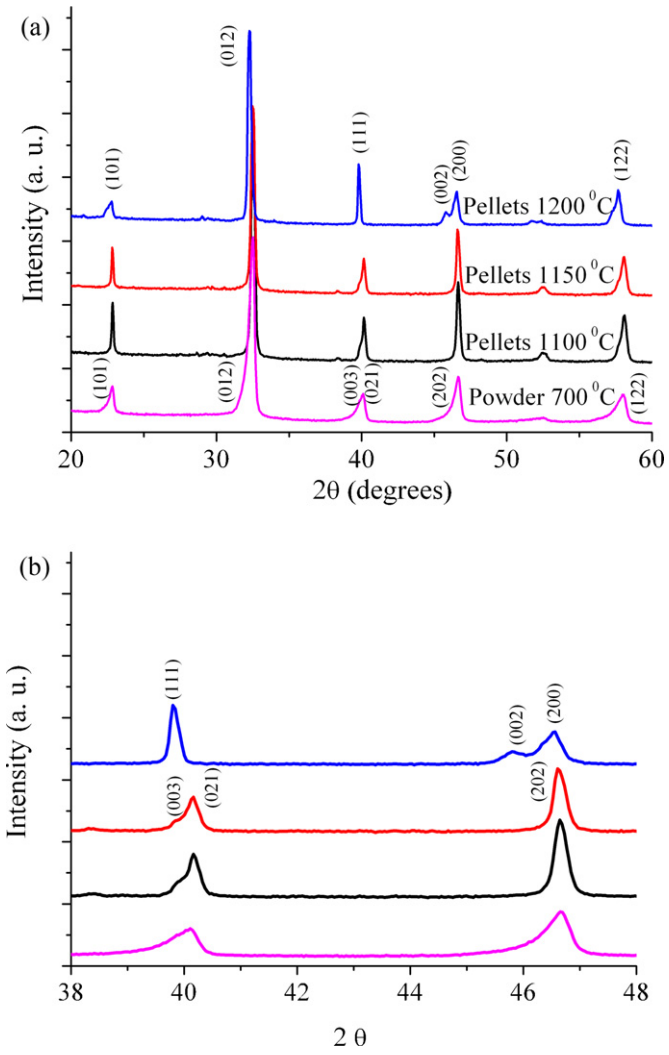

Fig. 3. X-ray diffraction patterns ($2\theta = 20$–$80°$) of $BaTiO_3$ doped-$Na_{1/2}Bi_{1/2}TiO_3$ powder and sintered pellets at 1100 and 1150 °C for 2 h, and 1200 °C, 1 h in air (a) and, XRD patterns of the powder and ceramics in the 2θ range of 38–48° (b).

crystal structure and properties of ferroelectric ceramics. For example, ultrafine $BaTiO_3$ (particles <0.12 μm) shows cubic and nonferroelectric structure, while $BaTiO_3$ powder with average grain size higher than 1.1 μm presents tetragonal ferroelectric structure.[30] The most widely considered possible causes for the cubic structure of very fine $BaTiO_3$ powder are the following: depolarization effects, absence of long-range interactions, structure defects and elastic constraints.[30] These considerations are valid for materials with perovskite structure, including NBT. The existence of the tetragonal phase in the NBT–$BT_{0.11}$ samples sintered at temperature higher than 1150 °C can be correlated with the increasing of grain average size over a certain threshold. Thus, the sample sintered at 1100 °C shows grains of 150 nm to 0.6 μm and rhombohedral structure, while the pellets sintered at 1200 °C exhibits grains of 400 nm to 1.5 μm and tetragonal symmetry. The crystallographic phase composition in NBT–BT_x depends on the temperature and/or chemical composition. The tetragonal phase of NBT–BT_x composition having $x = 0.11$,

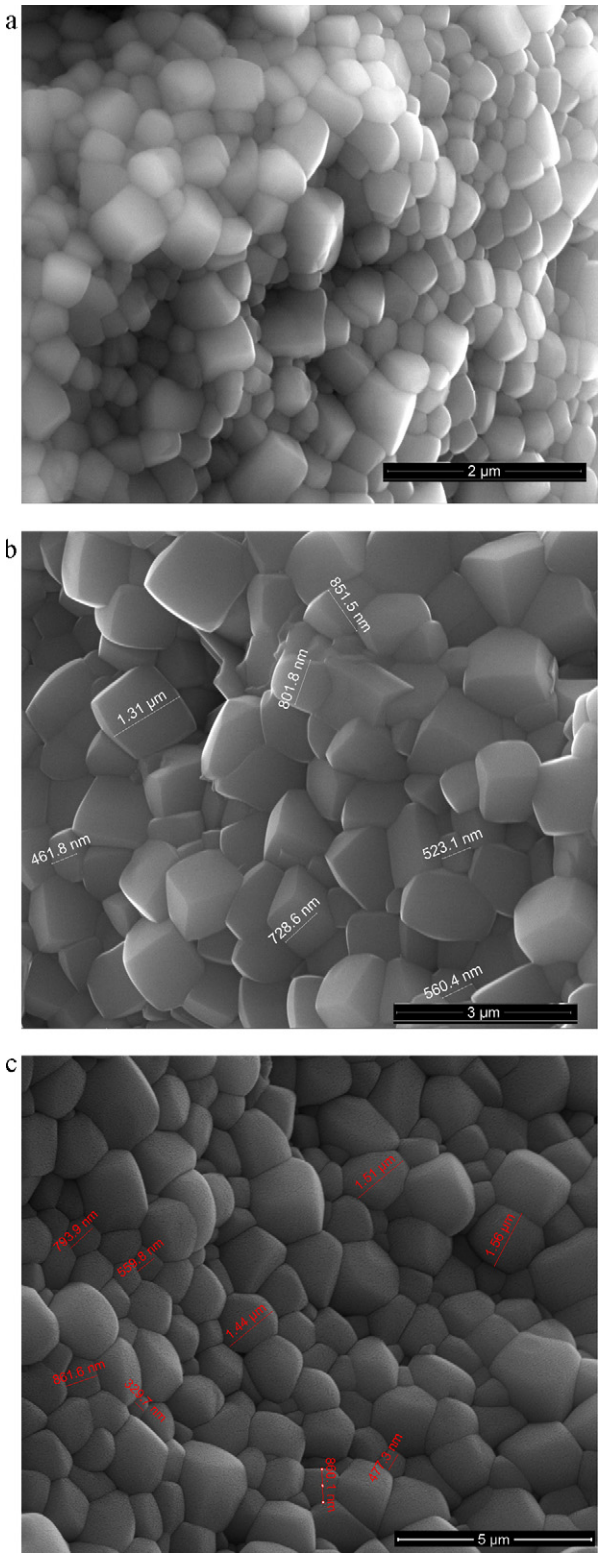

Fig. 4. SEM micrographs of the $BaTiO_3$ doped-$Na_{1/2}Bi_{1/2}TiO_3$ ceramic sintered at 1100 (a) and 1150 °C (b), 2 h in air and, 1200 °C (c), 1 h in air.

which is near the morphotropic phase boundary, was reported in the literature.[31] Therefore, in order to obtain a single NBT tetragonal phase for NBT–BT_x ceramics, it is necessary to add more than 10 mol% $BaTiO_3$ and a sintering temperature higher than 1150 °C.

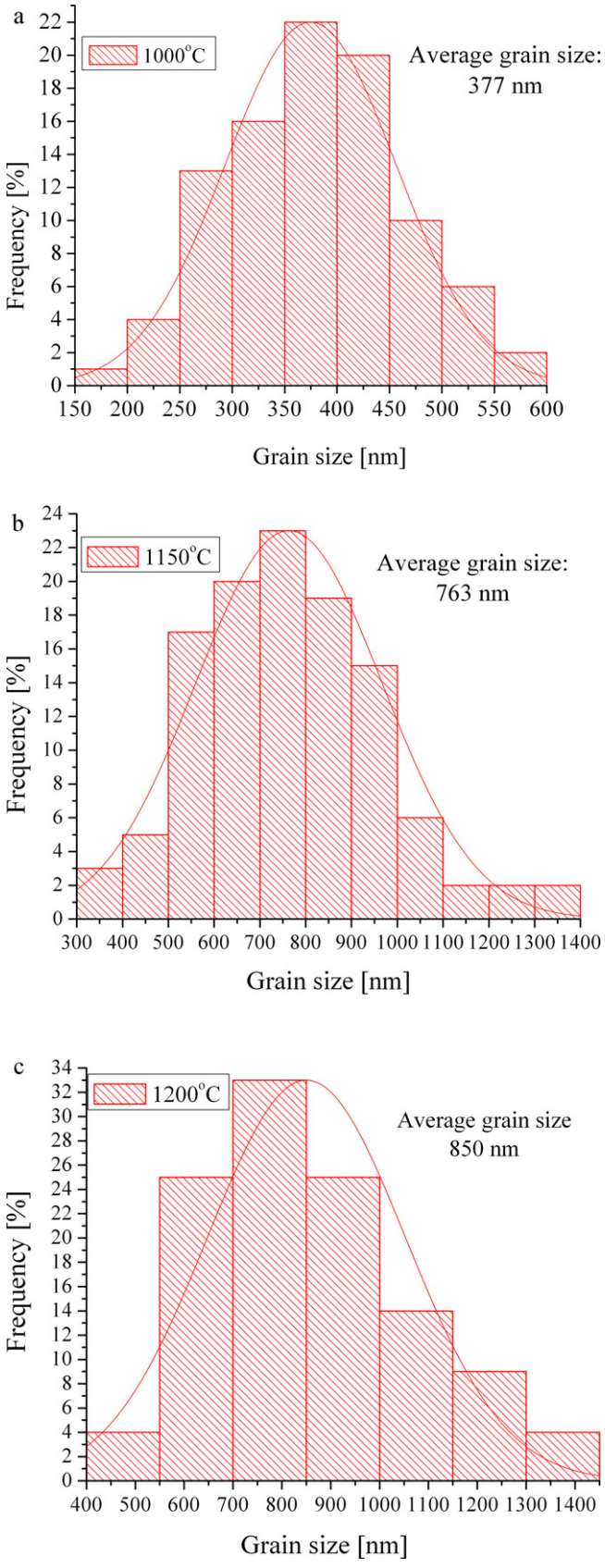

Fig. 5. The grain size distribution for NBT–$BT_{0.11}$ ceramics sintered at1100 °C (a), 1150 °C (b) and 1200 °C (c).

3.3. Sintering behavior and piezoelectric characterization

The SEM micrographs of the surface fractures and the grain size distribution for NBT–$BT_{0.11}$ ceramics sintered at1100 °C (a), 1150 °C (b) and 1200 °C (c) are shown in Figs. 4(a)–(c) and 5(a)–(c), respectively.

As shown in Fig. 4, the NBT–$BT_{0.11}$ grains are of polyhedral shape. The sample sintered at 1100 °C seems to be homogeneous for the grain size point of view; therefore, it exhibits a monomodal grain size distribution. In the case of NBT–$BT_{0.11}$ ceramic sintered at 1100 °C (Fig. 4(a)), the grain average size is 377 nm (Fig. 5(a)). A monomodal grain size distribution can be also noticed for the ceramics obtained after sintering at 1150 °C (Fig. 4(b)) and 1200 °C (Fig. 4(c)), with grain average size of 763 nm (Fig. 5(b)) and 850 nm (Fig. 5(c)), respectively. The dense and pore-free microstructures of all ceramic samples can be attributed to the homogeneous and fine morphology of the preliminary particles from the calcined powder.

The temperature dependence of dielectric properties measured at frequencies of 120 Hz, 1 kHz, 10 kHz, 100 kHz and 1 MHz for unpoled NBT–$BT_{0.11}$ ceramic is presented in Fig. 6.

Permittivity and loss values increase with the sintering temperature increasing (Fig. 6(a–c)). For 1100 °C sintering temperature, a more diffuse phase transition with low values of permittivity ($\varepsilon_r = 2538$ at 1 kHz; $\varepsilon_r = 2340$ at 100 kHz) and losses ($\tan\delta = 0.058$ at 1 kHz; $\tan\delta = 0.038$ at 100 kHz) can be observed in Fig. 6(a). The increase of the sintering temperature leads to increased values of permittivity, with maximum at 1200 °C ($\varepsilon_r = 5456$ at 100 kHz), having well defined peaks (Fig. 6(c)). In the investigated temperature range, permittivity values decrease with the frequency increasing. For example, NBT–$BT_{0.11}$ ceramic sintered at 1150 °C shows a dielectric constant value of $\varepsilon_r = 3742$ at T_m and 1 kHz, which decreases to $\varepsilon_r = 3557$ at 100 kHz. These considerations could be attributed to the rhombohedral structure with lower permittivity of NBT–$BT_{0.11}$ samples sintered at 1100 and 1150 °C and to a tetragonal structure with higher dielectric constant of the samples sintered at 1200 °C, in good agreement with the X-ray diffraction analysis (Fig. 3).[24]

Dielectric losses exhibit a more complex behavior, related to the samples temperature, but, generally, decrease with the frequency increasing. At low frequency value (120 Hz) and at temperatures above 225 °C, the losses exhibit an obvious increase that could be attributed to the thermal activated conductivity, generated by oxygen vacancies that form dipolar defects ($[V_{Bi}]^{3+}$–$[V_O]^{2-}$). The high conductivity of BNT ceramics is associated with Bi vaporization during sintering at temperatures $\geq$1130 °C.[32] Bi vaporization leads to the generation of $[V_{Bi}]^{3+}$, which is accompanied by the formation of $[V_O]^{2-}$ due to the charge compensation. Activation energy and relaxation time can be obtained by applying to our data (Fig. 6(c)) a similar analysis to the one reported in Ref. 33. The obtained numbers are 0.95 ± 0.1 eV for the activation energy and about $(0.3–0.4) \times 10^{-12}$ s for the relaxation time. Although the values are quite rough, they fit well the reported numbers for dipole defects associated to oxygen vacancies. Such dipoles can induce an internal electric field and an

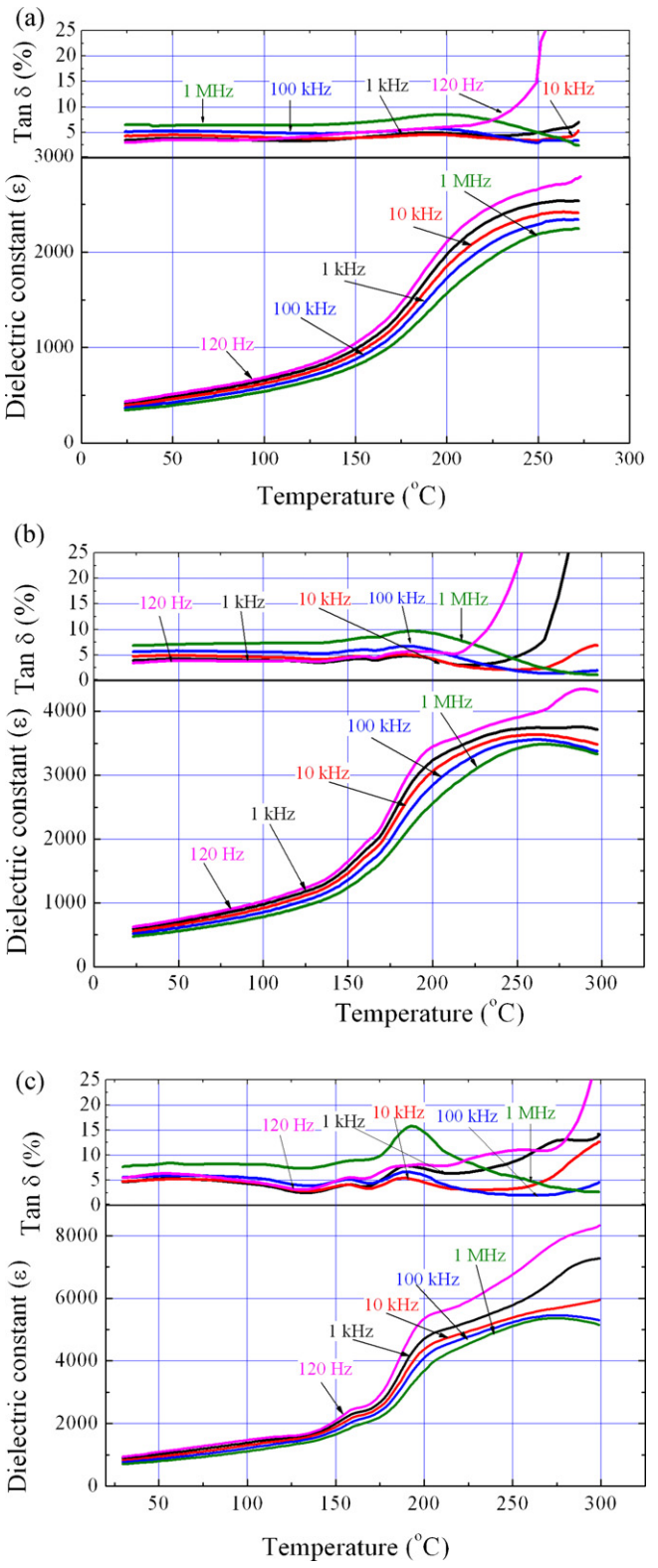

Fig. 6. Temperature and frequency dependence of dielectric constant and dielectric loss of unpoled NBT–$BT_{0.11}$ ceramic, sintered at 1100 °C (a), 1150 °C (b), and 1200 °C (c).

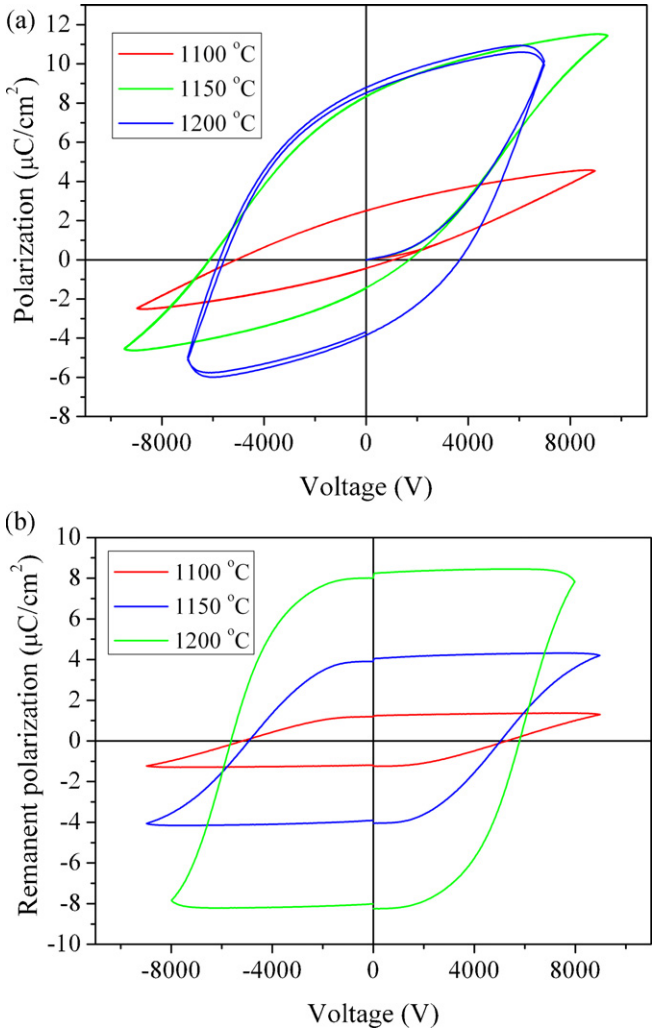

Fig. 7. Hysteresis loops for the NBT–$BT_{0.11}$ ceramics sintered at various temperatures (a) and pure ferroelectric hysteresis loop obtained by a procedure similar to the PUND method (b).

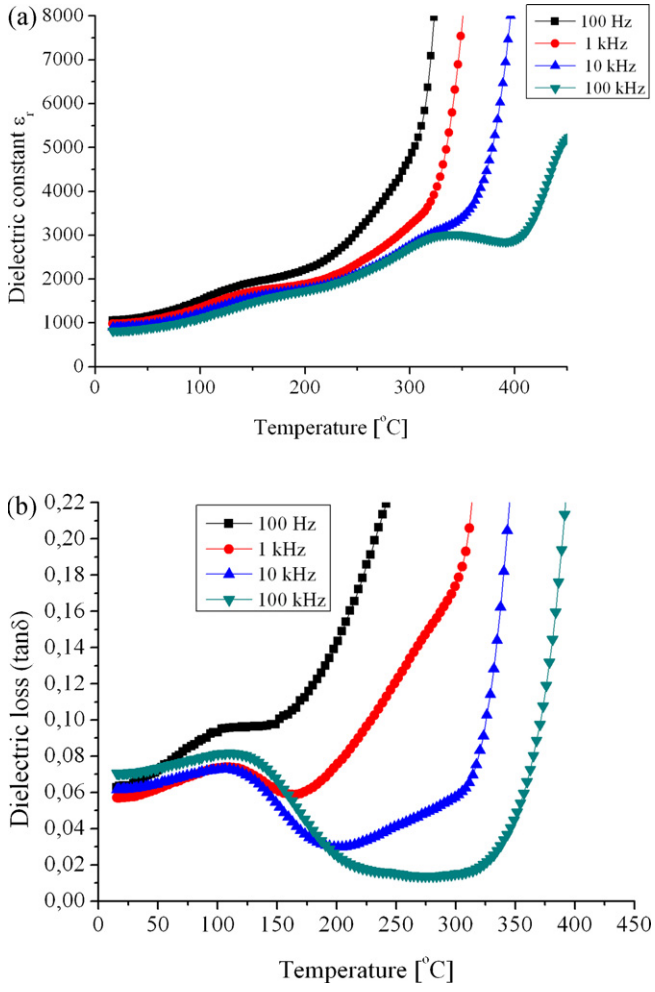

Fig. 8. Temperature and frequency dependence of dielectric constant (a) and dielectric loss (b) of NBT–$BT_{0.11}$ ceramic sintered at 1150 °C and poled.

offset polarization at lower temperatures. This was checked by performing hysteresis measurements at room temperature, were it was assumed that defect dipoles are still oriented parallel to the ferroelectric polarization. The obtained loop is shown in Fig. 7a only for the sample sintered at the highest temperature.

It can be seen that the loop is shifted up on the polarization axis, suggesting that the defect dipoles do not switch together with the ferroelectric polarization. They may orient parallel under the applied electric field, thus starting with positive voltage they orient parallel with the ferroelectric polarization but for negative voltage they do not switch. Therefore the negative remnant polarization is smaller than the positive one. In the same time the defect dipoles generate an internal field which helps the positive polarization and oppose to the negative one, thus the loop is shifted toward the negative values on the voltage axis. The pure ferroelectric hysteresis loop obtained by a procedure similar to the PUND method is presented in Fig. 7b. It can be seen that after extracting all the losses due to defects, leakage, *etc.* the loop is almost symmetric with a polarization value of approximately 8 μC/cm^2.

Fig. 8 shows temperature and frequencies dependence of the dielectric constant (a) and loss tangent (b) of NBT–$BT_{0.11}$ ceramic sintered at 1150 °C, for 2 h, and poled from room temperature to 450 °C.

The relative permittivity at room temperature of unpoled ($\varepsilon_r = 1000$) and poled ($\varepsilon_r = 924$) NBT–$BT_{0.11}$ processed by sol–gel is smaller than that of unpoled ($\varepsilon_r = 1600$) and poled ($\varepsilon_r = 1200$) NBT–$BT_{0.11}$ produced by the conventional solid state reaction method,[34] due to the smaller grains (763–850 nm) and domain structure. The average grain size of NBT–$BT_{0.11}$ ceramic samples prepared by a solid oxide route[34] was about 2 μm.

As we can see from Figs. 6 and 8, the curves present three distinct regions, divided by two special temperatures (T_d and T_m). The temperature at which the phase transition between the ferroelectric rhombohedral phase and the pseudocubic phase[21] happens is called depolarization temperature (T_d), while the temperature corresponding to the maximum value of the dielectric constant is named maximum temperature (T_m). At these

Table 1
Piezoelectric and ferroelectric properties of BNT–$BT_{0.11}$ ceramics sintered at 1150 °C and poled, compared with published values for BNT–BT_x.

Properties		This paper	Ref. 24	Ref. 27; $x=0.08$	Ref. 31; $x=0.05$
Electromechanical coupling factors	k_p	0.035	0.27, $x=0.04$; 0.28, $x=0.06$	0.047	0.091
	k_{31}	−0.021		−0.029	−0.055
	k_t	0.034		0.074	0.105
Frequency constants	N_p [m/s]	2784		2890	2923
	N_t [m/s]	2246		2051	2329
Piezoelectric charge coefficient	d_{31} [pC/N]	−6.40		−8.96	−16.62
	d_{33} [pC/N]	13	118, $x=0.04$; 142, $x=0.06$	26	77
Piezoelectric voltage coefficient	g_{31} [10^{-3} Vm/N]	−0.782		−0.869	−1.738
	g_{33} [10^{-3} Vm/N]	1.644		2.489	8.100
Dielectric loss	$\tan\delta$	0.057		0.02	0.045
Dielectric constant	ε_{33}^{T}	924		1164	1080
	ε_{33}^{S}	922		1155	1060
Elastic stiffness	c_{33}^{D} [10^{10} N/m^2]	10.51		9.45	12.17
	c_{33}^{D} [10^{10} N/m^2]	10.52		9.50	12.17
Elastic compliance	s_{11}^{E} [10^{-12} m^2/N]	10.98		9.53	9.58
	s_{12}^{E} [10^{-12} m^2/N]	−2.823		−2.51	−2.665
Mechanical quality factor	Q_m	860.32		482.4	197.5
Poisson factor	σ^{E}	0.2571		0.2637	0.2782
Sonic velocity	v_1^{E} [m/s]	4181			4334
Acoustic impedance	Z_a [10^6 kg/(m^2 s)]	21.78			24.09
Temperature of maximum of dielectric constant	T_m (°C)	261		.	342
Depolarization temperature	T_d (°C)	110			139

temperatures, the dielectric characteristics are frequency dependent, which shows that the NBT–$BT_{0.11}$ ceramics are ferroelectric relaxors. Depolarization temperature, which has been suggested to be an indication of the stability of the ferroelectric domains,[21] plays an important role in the practical application of NBT-based materials. T_d can be derived from the temperature of $\tan\delta$ first peak of the poled specimens.[9] From Fig. 8(b), we can see that T_d has a small variation with frequency and its value is ∼110 °C. The temperature of dielectric constant maximum (T_m) was appreciated from Fig. 6(b) at about 260 °C (at 1 kHz) because, in Fig. 8(a) T_m is not distinctive. Fig. 6 shows that T_m decreases as sintering temperature increases ($T_m = 264$ °C for the ceramic sintered at 1100 °C and $T_m = 261.7$ °C for the ceramic sintered at 1150 °C), and T_m increases with frequency increasing (for example, $T_m = 260.6$ °C at 1 kHz and $T_m = 261.7$ °C at 100 kHz for the ceramic sintered at 1150 °C).

A third transition temperature (around 200 °C) appears on the permittivity curves of samples sintered at 1150 and 1200 °C (Fig. 6(a) and (b)). Some authors described this intermediate phase as a rhombohedral/tetragonal coexisting phase from the results of second-harmonic generation and the observation of birefringence imaging using BNT single crystals.[35,36] Vakhrushev et al.[37] described that the intermediate phase is nonpolar, and optical isotropization has been observed in the literature.[36–38] This intermediate phase is traditionally thought to be antiferroelectric owing to the observation of doublelike hysteresis loops in BNT-based solid solutions[39] however, the nature of this intermediate phase has not yet been clarified completely. Watanabe et al.[40] called this third transition temperature as rhombohedral/tetragonal phase transition temperature (T_{r-t}) and suggested the existence of a morphotrophic phase boundary.[41] Hiruma et al.[42] verified a very small tetragonal distortion in pure BNT above this T_{r-t}, which supports Watanabes hypothesis.

As shown in Fig. 6, the higher dielectric constant peaks at T_m are relatively broad for all ceramics, suggesting that the phase transition at T_m is a diffuse one. The diffuse phase transition has been observed in many ABO_3-type perovskites and NBT-based ceramics,[43] in which either the A-sites or the B-sites are occupied by at least two cations. The dielectric behavior of complex ferroelectrics with diffuse phase transition can be explained by the modified Curie–Weiss law[44]:

$$\frac{1}{\varepsilon_r} - \frac{1}{\varepsilon_m} = \frac{(T - T_m)^{\gamma}}{C'}, \quad (1)$$

where ε_m is the maximum value of the permittivity, T_m is the temperature at which ε reaches the maximum, C' is the Curie-like constant and γ ($1 < \gamma < 2$) is a constant which is used to express the diffuseness degree of the phase transition. When $\gamma = 1$, the materials with this type of phase transition belong to normal ferroelectrics; when $1 < \gamma < 2$, the materials belong to relaxor ferroelectrics; when $\gamma = 2$, the materials belong to ideal relaxor ferroelectric. Plots of $\ln(1/\varepsilon_r - 1/\varepsilon_m)$ as a function of $\ln(T - T_m)$, at 100 kHz, for NBT–$BT_{0.11}$ ceramics sintered at 1100–1200 °C are shown in Fig. 9.

The experimental dielectric constant data were fitted with Eq. (1) in the vicinity of T_m. The obtained γ values were 1.80, 1.90 and 1.99 for the sample sintered at 1100, 1150 and 1200 °C, respectively. The diffuseness exponent (γ) of the NBT–$BT_{0.11}$ ceramics is between 1 and 2, which confirms that the phase

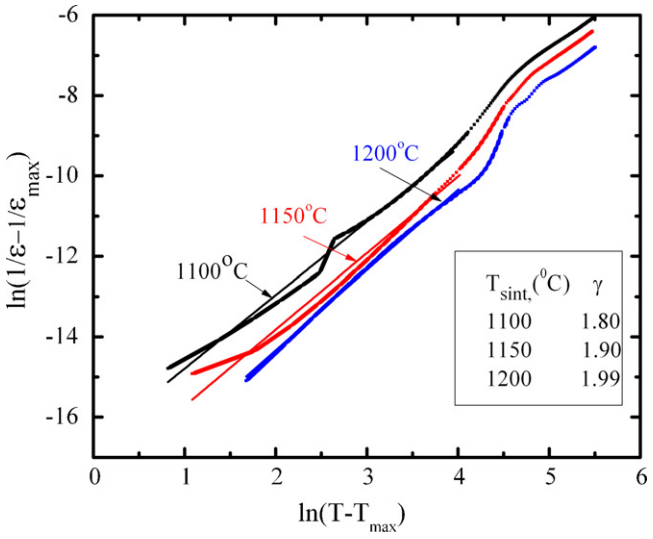

Fig. 9. Dielectric permittivity data fitted with modified Curie–Weiss law for NBT–$BT_{0.11}$ ceramics sintered at various temperatures.

transition of these ceramics is diffuse, in good accordance with Figs. 6 and 8.

The results of the piezoelectric characterization of the poled NBT–$BT_{0.11}$ ceramic sintered at 1150 °C, for 2 h, measured at room temperature and at resonant frequency, are listed in Table 1.

Compared with the results reported previously for NBT–BT_x ceramics with $x = 0.05$, 0.06 and 0.08,[24,27,45] our NBT–$BT_{0.11}$ ceramic shows smaller values for the electromechanical coupling factor (k_p), piezoelectric charge coefficient (d_{33}), piezoelectric voltage coefficient (g_{33}) and dielectric constant (ε_{33}), and higher values for the mechanical quality factor (Q_m). NBT–$BT_{0.11}$ ceramics exhibit properties comparable to those of our NBT–$BT_{0.08}$ ceramics prepared by sol–gel,[21] but slightly smaller values for k_p, d_{33}, g_{33} and ε_{33}, and slightly greater values for Q_m. The NBT–$BT_{0.11}$ ceramics derived from sol–gel have higher mechanical quality factor ($Q_m = 860$) and dielectric permittivity ($\varepsilon_{33} = 922$–924) than other materials reported in the literature.[11] The piezoelectric coefficient exhibits a higher value of 120 pC/N at poled NBT–$BT_{0.11}$ produced by the conventional solid state reaction method[34] than that $d_{33} = 13$ pC/N of our NBT–$BT_{0.11}$ processed by sol–gel.

These results show that grain size is an important microstructural characteristic that affects piezo-electric properties. Although the piezoelectric properties degrade with smaller grain size, and improved the mechanical strength and dielectric strength.[46] Several models, including the presence of internal stresses in fine-grained ceramics, which are due to the absence of 90 domain walls, increased domain-wall contributions to the dielectric response in fine-grained ceramics, shifts of the phase transition temperatures with grain size have been considered.[47]

4. Conclusions

$Na_{1/2}Bi_{1/2}TiO_3$ doped with 11 mol% $BaTiO_3$ lead-free piezoelectric ceramics have been synthesized by sol–gel process. The crystalline phases, microstructure, dielectric and piezoelectric properties of the obtained ceramics have been investigated. XRD data indicates that the ceramics sintered at temperatures up to 1150 °C have a rhombohedral structure and those sintered at 1200 °C have a tetragonal symmetry. The powder prepared by sol–gel technique is composed of nanoparticles and agglomerates; the crystallite average size is around 50 nm. The temperature dependence of the dielectric constant and loss tangent of NBT–$BT_{0.11}$ ceramics reveals that the T_d temperature remains almost constant with the frequency variation. The NBT–$BT_{0.11}$ ceramics exhibit diffuse phase transition and relaxor behavior. The degree of diffuseness increases with the sintering temperature increasing. NBT–$BT_{0.11}$ ceramics show high mechanical quality factor, high dielectric characteristics and low piezoelectric properties. The high mechanical quality factor of NBT–$BT_{0.11}$ ceramics recommends them as ceramic resonator. The dielectric and piezoelectric properties values of NBT–$BT_{0.11}$ ceramics derived from sol–gel are smaller than those of samples produced by the conventional solid state reaction method, due to the grains size and oxygen vacancies that generate dipolar defects. The grain average size values of the samples produced by the conventional solid state reaction method are in the micron range, while the NBT–$BT_{0.11}$ ceramics investigated in this work, present grain average size values in the submicron range. According to the current knowledge, a significant influence of the reduced grain size on the dielectric and piezoelectric properties is expected, with a substantial decrease of d_{33}.

Acknowledgment

The authors gratefully acknowledge the Romanian Research Ministry PNCDI II, Contract No. 72-153/2008, for financial support.

References

1. Haertling GH. Ferroelectric ceramics: history and technology. *J Am Ceram Soc* 1999;**82**:797–818.
2. Zhang SJ, Xia R, Lebrun L, Anderson D, Shrout TR. Piezoelectric materials for high power, high temperature applications. *Mater Lett* 2005;**59**:3471–5.
3. Yuan J, Wang DW, Lin HB, Zhao QL, Zhang DQ, Cao MS. Effect of ZnO whisker content on sinterability and fracture behaviour of PZT peizoelectric composites. *J Alloy Compd* 2010;**504**:123–8.
4. Cao MS, Wang DW, Yuan J, Lin HB, Zhao QL, Song WL, Zhang DQ. Enhanced piezoelectric and mechanical properties of ZnO whiskers and Sb_2O_3 co-modified lead zirconate titanate composites. *Mater Lett* 2010;**64**:1798–801.
5. Wang DW, Cao MS, Yuan J, Zhao QL, Lin HB, Zhang DQ, Agathopoulos S. Enhanced piezoelectric and ferroelectric properties of Nb_2O_5 modified lead zirconate titanate-based composites. *J Am Ceram Soc* 2011;**94**:647–50.
6. Zhang DQ, Qin ZC, Yang XY, Zhu HB, Cao MS. Study on synthesis and evolution of sodium potassium niobate ceramic powders by an oxalic acid-based sol–gel method. *J Sol–Gel Sci Technol* 2011;**57**:31–5.
7. Xu C, Lin D, Structure Kwok KW. electrical properties and depolarization temperature of $(Bi_{0.5}Na_{0.5})TiO_3$–$BaTiO_3$ lead-free piezoelectric ceramics. *Solid State Sci* 2008;**10**:934–40.
8. Herabut A, Safari A. Processing and electromechanical properties of $(Bi_{0.5}Na_{0.5})_{0.99}Ca_{1-1.5x}La_xTiO_3$ ceramics. *J Am Ceram Soc* 1997;**80**:2954–8.
9. Hiruma Y, Nagata H, Takenaka T. Phase transition temperatures and piezoelectric properties of $(Bi_{1/2}Na_{1/2})TiO_3$–$(Bi_{1/2}K_{1/2})TiO_3$–$BaTiO_3$ lead-free piezoelectric ceramics. *Jpn J Appl Phys* 2006;**45**:7409–12.

10. Zhao S, Li G, Ding A, Wang T, Rui Q. Ferroelectric and piezoelectric properties of $(Na,K)_{0.5}Bi_{0.5}TiO_3$ lead free ceramics. *J Phys D: Appl Phys* 2006;**39**:2277–81.
11. Li YM, Chen W, Zhou J, Xu Q, Sun HJ, Xu RX. Dielectric and piezoelectric properties of lead-free $(Na_{0.5}Bi_{0.5})TiO_3$–$NaNbO_3$ ceramics. *Mater Sci Eng B* 2004;**112**:5–9.
12. Wang XX, Tang XG, Kwok K, Chan HLW, Choy CL. Effect of excess Bi_2O_3 on the electrical properties and microstructure of $(Bi_{1/2}Na_{1/2})TiO_3$ ceramics. *Appl Phys A* 2005;**80**:1071–5.
13. Lin D, Xiao D, Zhu J, Yu P. Piezoelectric and ferroelectric properties of $[Bi_{0.5}(Na_{1-x-y}K_xLi_y)_{0.5}]TiO_3$ lead-free piezoelectric ceramics. *Appl Phys Lett* 2006;**88**:062901–3.
14. Lin D, Xiao D, Zhu J, Yu P. Piezoelectric and ferroelectric properties of lead-free $[Bi_{1-y}(Na_{1-x-y}Li_x)]_{0.5}Ba_yTiO_3$ ceramics. *J Eur Ceram Soc* 2006;**26**:3247–51.
15. Li YM, Chen W, Xu Q, Zhou J, Gu X, Fang S. Thermal annealing effect on Y_2O_3:Eu^{3+} phosphor films prepared by yttrium 2-methoxyethoxide sol–gel precursor. *Mater Chem Phys* 2005;**94**:328–32.
16. Shieh J, Wu KC, Chen CS. Switching characteristics of MPB compositions of $(Bi_{0.5}Na_{0.5})TiO_3$–$BaTiO_3$–$(Bi_{0.5}K_{0.5})TiO_3$ lead-free ferroelectric ceramics. *Acta Mater* 2007;**55**:3081–7.
17. Zhang S, Shrout TR, Nagata H, Hiruma Y, Takenaka T. Piezoelectric properties in $(K_{0.5}Bi_{0.5})TiO_3$–$(Na_{0.5}Bi_{0.5})TiO_3$–$BaTiO_3$ lead-free ceramics. *IEEE Trans Ultrason Ferroelectr Freq Control* 2007;**54**:910–7.
18. Chu BJ, Chen DR, Li GR, Yin QR. Effect of A-site substitution on crystal component and dielectric properties in $Na_{0.5}Bi_{0.5}TiO_3$ ceramics. *J Eur Ceram Soc* 2002;**22**:2115–21.
19. Ranjan R, Dviwedi A. Structure and dielectric properties of $(Na_{0.50}Bi_{0.50})_{1-x}Ba_xTiO_3$: $0 \le x \le 0.10$. *Solid State Commun* 2005;**135**:394–9.
20. Zhou XY, Gu HS, Wang Y, Li WY, Zhou TS. Piezoelectric properties of Mn-doped $(Na_{0.5}Bi_{0.5})_{0.92}Ba_{0.08}TiO_3$ ceramics. *Mater Lett* 2005;**59**:1649–52.
21. Takenaka T, Maruyama KI, Sakata K. $(Na_{1/2}Bi_{1/2})TiO_3$–$BaTiO_3$ system for lead-free piezoelectric ceramics. *Jpn J Appl Phys* 1991;**30**:2236–9.
22. West DL, Payne DA. Preparation of $0.95(Na_{1/2}Bi_{1/2})TiO_3$–$0.05BaTiO_3$ ceramics by an aqueous citrate–gel rout. *J Am Ceram Soc* 2003;**86**:192–4.
23. Chen M, Xu Q, Kim BH, Ahn BK, Ko JH, Kang WJ, Nam OJ. Structure and electrical properties of $(Na_{0.5}Bi_{0.5})_{1-x}Ba_xTiO_3$ piezoelectric ceramics. *J Eur Ceram Soc* 2008;**28**:843–9.
24. Kim BH, Han SJ, Kim JH, Lee JH, Ahn BK, Xu Q. Electrical properties of $(1-x)(Na_{1/2}Bi_{1/2})TiO_3$–$xBaTiO_3$ synthesized by emulsion method. *Ceram Int* 2007;**33**:447–52.
25. Pookmanee P, Rujijanagul G, Ananta S, Heimann RB, Phanichphant S. Effect of sintering temperature on microstructure of hydrothermally prepared bismuth sodium titanate ceramics. *J Eur Ceram Soc* 2004;**24**:517–20.
26. Mercadelli E, Galassi C, Costa AL, Albonetti S, Sanson A. Sol–gel combustion synthesis of NBBT powders. *J Sol–Gel Sci Technol* 2008;**46**:39–45.
27. Cernea M, Andronescu E, Radu R, Fochi F, Galassi C. Sol–gel synthesis and characterization of $BaTiO_3$ doped-$(Na_{1/2}Bi_{1/2})TiO_3$ piezoelectric ceramics. *J Alloy Compd* 2010;**490**:690–4.
28. Hao J, Wang XH, Chen RZ, Li LT. Synthesis of $Na_{0.5}Bi_{0.5}TiO_3$ nanocrystalline powders by stearic acid gel method. *Mater Chem Phys* 2005;**90**:282–5.
29. Jones GO, Thomas PA. *Acta Crystallogr Sect B: Struct Sci* 2002;**58**:168 [Pattern: 01-070-9850].
30. Frey MH, Payne DA. Grain-size effect on structure and phase transformations for barium titanate. *Phys Rev B* 1996;**54**:3158–67.
31. Trujillo S, Kreisel J, Jiang Q, Smith JH, Thomas PA, Bouvier P, Weiss F. The high-pressure behaviour of Ba-doped $Na_{0.5}Bi_{0.5}TiO_3$ investigated by Raman spectroscopy. *J Phys: Condens Matter* 2005;**17**:6587–97.
32. Nagata H, Shinya T, Hiruma Y, Takenaka T, Sakaguchi I, Haneda H. Piezoelectric properties of bismuth sodium titanate ceramics. *Ceram Trans* 2005;**167**:213–22.
33. Zhou L, Huiqing F. Relaxation associated with the synergetic oxygen vacancies and electrons in $(Ba_{1-x}Bi_x)_{0.9}Sr_{0.1}TiO_{3-\delta}$ ceramics. *J Appl Phys* 2010;**108**:034103–9.
34. Jo W, Daniels JE, Jones JL, Tan X, Thomas PA, Damjanovic D, Roedel J. Evolving morphotropic phase boundary in lead-free $(Bi_{1/2}Na_{1/2})TiO_3$–$BaTiO_3$ piezoceramics. *J Appl Phys* 2011;**109**:014110.
35. Jones GO, Thomas PA. Investigation of the structure and phase transitions in the novel A-site substituted distorted perovskite compound $Na_{0.5}Bi_{0.5}TiO_3$. *Acta Crystallogr Sect B: Struct Sci* 2002;**58**:168–78.
36. Geday M, Kreisel J, Glazer AM, Roleder K. Birefringence imaging of phase transitions: application to $Na_{0.5}Bi_{0.5}TiO_3$. *J Appl Crystallogr* 2000;**33**:909–14.
37. Vakhrushev SB, Isupov VA, Kvyatkovsky BE, Okuneva NM, Pronin IP, Smolensky GA, Syrnikov PP. Phase transitions and soft modes in sodium bismuth titanate. *Ferroelectrics* 1985;**63**:153–60.
38. Park SE, Chung SJ, Kim IT, Hong KS. Nonstoichiometry and the long-range cation ordering in crystals of $(Na_{1/2}Bi_{1/2})$ TiO_3. *J Am Ceram Soc* 1994;**77**:2641–7.
39. Sakata K, Masuda Y. Ferroelectric and antiferroelectric properties of $(Na_{0.5}Bi_{0.5})TiO_3$–$SrTiO_3$ solid solution ceramics. *Ferroelectrics* 1974;**7**:347–9.
40. Watanabe Y, Hiruma Y, Nagata H, Takenaka T. Phase transition temperature and electrical properties of divalent ions (Ca^{2+}, Sr^{2+} and Ba^{2+}) substituted $(Bi_{1/2}Na_{1/2})TiO_3$ ceramics. *Ceram Int* 2008;**34**:761–4.
41. Krauss W, Schütz D, Mautner FA, Feteira A, Reichmann K. Piezoelectric properties and phase transition temperatures of the solid solution of $(1-x)(Bi_{0.5}Na_{0.5})TiO_3$–$xSrTiO_3$. *J Eur Ceram Soc* 2010;**30**:1827–32.
42. Hiruma Y, Nagata H, Takenaka T. Thermal depoling process and piezoelectric properties of bismuth sodium titanate ceramics. *J Appl Phys* 2009;**105**:084112–84118.
43. Li YM, Chen W, Xu Q, Zhou J, Gu X, Fang S. Electromechanical and dielectric properties of $Na_{0.5}Bi_{0.5}TiO_3$–$K_{0.5}Bi_{0.5}TiO_3$–$BaTiO_3$ lead-free ceramics. *Mater Chem Phys* 2005;**94**:328–32.
44. Ukino K, Nomura S. Critical exponents of the dielectric constants in diffused-phase-transition crystals. *Ferroelectr Lett Sect* 1982;**44**:55–61.
45. Cernea M, Vasile BS, Capiani C, Ioncea A, Galassi C. Dielectric and piezoelectric behaviors of BNT–$BT_{0.05}$ processed by sol–gel method. *J Eur Ceram Soc* 2012;**32**:133–9.
46. McNeal MP, Jang SJ, Newnham RE. The effect of grain and particle size on the microwave properties of barium titanate ($BaTiO_3$). *J Appl Phys* 1998;**83**:3288–97.
47. Damjanovic D. Ferroelectric, dielectric and piezoelectric properties of ferroelectric thin films and ceramics. *Rep Prog Phys* 1998;**61**:1267–324.